RSC Advances

PAPER

Cite this: *RSC Adv.*, 2022, **12**, 14268

Impact of sp^2 carbon material species on Pt nanoparticle-based electrocatalysts produced by one-pot pyrolysis methods with ionic liquids†

Yu Yao,[ab] Qingning Xiao,[a] Masafumi Kawaguchi,[a] Tetsuya Tsuda, *[ac] Hirohisa Yamada[b] and Susumu Kuwabata*[ad]

Received 28th February 2022
Accepted 2nd May 2022

DOI: 10.1039/d2ra01330d

rsc.li/rsc-advances

Pt-nanoparticle-supported graphene nanoplatelets (Pt/GNPs) and multiwalled carbon nanotube composite (Pt/MWCNTs) electrocatalysts for the oxygen reduction reaction (ORR) can be prepared using a one-pot method through the pyrolytic decomposition of the platinum precursor, platinum(II) bis(acetylacetonate) ($Pt(acac)_2$) in 1-butyl-3-methylimidazolium bis(trifluoromethylsulfonyl)amide ($[C_4mim][Tf_2N]$) or *N*,*N*,*N*-trimethyl-*N*-propylammonium bis(trifluoromethanesulfonyl)amide ($[N_{1,1,1,3}][Tf_2N]$) ionic liquids (ILs) with the target sp^2 carbon support. In this one-pot pyrolysis method, which does not require any reagents to reduce Pt metal precursors or stabilize Pt nanoparticles, Pt nanoparticles are readily immobilized onto the sp^2 surface by a thin IL layer formed at the interface, which can work as a binder. We used three types of sp^2 carbon materials with different geometric shapes (graphene nanoplatelets with <3 (GNPs-3) and 18–24 layers (GNPs-20) and multiwalled carbon nanotubes (MWCNTs)) to investigate Pt nanoparticle formation and anchoring. All the electrocatalysts, especially Pt/MWCNTs, showed higher durability than the commercial catalyst owing to the combined effect of the IL binder and sp^2 carbon materials. Our findings strongly suggest that the original carbon surface properties are also an important factor for creating high-performance ORR electrocatalysts.

1. Introduction

Rationally designed Pt-nanoparticle-supported carbon (Pt/C) electrocatalysts have been used to expedite the sluggish oxygen reduction reaction (ORR) on the cathode for polymer membrane electrolyte fuel cells (PEMFCs), which are clean and high-power density solutions for powering vehicles.[1,2] However, such Pt/C catalysts are required to further reduce the overpotential for the ORR and increase the durability. The latter is regarded as an unavoidable issue owing to the dissolution[3] and Ostwald ripening[4] of Pt nanoparticles under harsh operating conditions. In addition, catalyst degradation is induced by carbon support corrosion. The most commonly used carbon support is carbon black (*e.g.*, Vulcan® X72), which has a high specific surface area and many functional groups that can easily anchor Pt nanoparticles. Unfortunately, carbon black is gradually oxidized and deformed during PEMFC operation, especially during start-up and shut-down.[5–8] This aggravates Pt detachment and aggregation. sp^2-hybridized carbon materials composed of two-dimensional hexagonal carbon planes such as carbon nanotubes (CNTs) and graphene analogs, *e.g.*, graphene nanoplatelets (GNPs), have emerged as promising candidates to replace the widely used carbon black in PEMFC catalysts. These materials have attracted considerable attention in recent years owing to their unique physicochemical properties, including excellent electrical and thermal conductivities, high corrosion resistance, and large specific surface area.[9,10] The application of corrosion-resistant carbon materials substantially reduces Pt nanoparticle-related carbon oxidation and degradation.[5,11–13] However, anchoring Pt nanoparticles onto the smooth and chemically inert surface of sp^2 carbon materials is difficult. In most cases, the honeycomb sp^2 structure is destroyed by the addition of functional groups when immobilizing Pt nanoparticles onto carbon materials[14,15] and heteroatoms are embedded into the sp^2 structure.[16,17] These approaches are accompanied by a high risk of lowering the expected stability of CNTs and GNPs. Wrapping a carbon surface with a polymer, which is categorized as a physical conjunction method, is another approach to fixing Pt nanoparticles onto the surface.[18,19] We have previously reported a similar concept, but using an ionic liquid (IL) as the binder.[20–22] In this manner, highly

[a]*Department of Applied Chemistry, Graduate School of Engineering, Osaka University, 2-1 Yamada-oka, Suita, Osaka 565-0871, Japan. E-mail: ttsuda@chiba-u.jp; kuwabata@chem.eng.osaka-u.ac.jp*

[b]*Department of Chemical Engineering, National Institute of Technology, Nara College, 22 Yata-cho, Yamatokoriyama, Nara 639-1080, Japan*

[c]*Department of Materials Science, Graduate School of Science and Engineering, Chiba University, 1-33 Yayoicho, Inage-ku, Chiba 263-8522, Japan*

[d]*Innovative Catalysis Science Division, Institute for Open and Transdisciplinary Research Initiatives, Osaka University, 2-1 Yamada-oka, Suita, Osaka 565-0871, Japan*

† Electronic supplementary information (ESI) available. See https://doi.org/10.1039/d2ra01330d

Table 1 Preparation conditions and characterization data for specimens 1–6 and Pt–C

Specimens	Ionic liquids[a]	Carbon materials	Mean particle size/nm	Pt loading amount/wt%
1	$[C_4mim][Tf_2N]$	GNPs-3	2.1 (0.3)[b]	25.4
2	$[C_4mim][Tf_2N]$	GNPs-20	2.5 (0.5)[b]	25.0
3	$[C_4mim][Tf_2N]$	MWCNTs	2.7 (0.5)[b]	26.5
4	$[N_{1,1,1,3}][Tf_2N]$	GNPs-3	3.3 (0.5)[b]	25.5
5	$[N_{1,1,1,3}][Tf_2N]$	GNPs-20	3.8 (0.5)[b]	24.5
6	$[N_{1,1,1,3}][Tf_2N]$	MWCNTs	4.3 (0.7)[b]	25.3
Pt–C	—	—	2.6 (0.7)[26]	23.7 (ref. 26)

[a] 5 mmol L^{-1} $Pt(acac)_2$ was added as a Pt metal precursor. [b] Values in parentheses are standard deviations.

durable Pt/C electrocatalysts for the ORR are easily produced by heating and/or agitating the Pt-nanoparticle-dispersed IL with the carbon support.[23–25] In electrocatalysts, small quantities of the IL, which can remain even after electrochemical cleaning, impede direct contact between Pt nanoparticles and the carbon surface, thereby inhibiting carbon support corrosion.

Inspired by this approach, we recently established a simple and mass-producible one-pot pyrolysis method with IL (IL one-pot pyrolysis method) for preparing composite Pt and PtNi alloy-nanoparticle-supported multiwalled carbon nanotube composite (MWCNT) electrocatalysts for the ORR.[26] Unlike commonly used colloid methods, wherein the size and shape of nanoparticles are directly controlled by capping, stabilizing, and reducing agents,[27–29] no additional agents are needed for the IL one-pot pyrolysis method. In this study, to investigate the impact of sp^2 carbon material species on the ORR performance of electrocatalysts, we applied this IL one-pot pyrolysis method to graphene-based carbon materials, graphene nanoplatelets with <3 (GNPs-3) and 18–24 layers (GNPs-20) and MWCNTs. Using two types of ILs, 1-butyl-3-methylimidazolium bis(trifluoromethylsulfonyl)amide ($[C_4mim][Tf_2N]$) and *N*,*N*,*N*-trimethyl-*N*-propylammonium bis(trifluoromethanesulfonyl) amide ($[N_{1,1,1,3}][Tf_2N]$), we revealed the key factors responsible for controlling and maintaining the Pt nanoparticle size, which are directly related to the electrocatalytic performance.

2. Experimental

2.1 Preparation of the specimens

We prepared all specimens by a one-pot pyrolytic process under an N_2 atmosphere. The reaction medium for the one-pot process was composed of 2 mL IL ($[C_4mim][Tf_2N]$ (Kanto Chemical Co., Inc.) or $[N_{1,1,1,3}][Tf_2N]$ (Kanto Chemical Co., Inc.), Fig. S1 (ESI†)), 5 mmol L^{-1} platinum(II) bis(acetylacetonate) ($Pt(acac)_2$ (Mitsuwa Chemicals Co., Ltd.)), and 1.25 g L^{-1} of sp^2 carbon materials. The carbon materials were graphene powder (Sigma-Aldrich Co., LLC., thickness: <3 graphene layers; lateral size: 0.5–5 μm (GNPs-3)), graphene nanoplatelets (Strem Chemical Co., Inc., thickness: 6–8 nm (18–24 graphene layers); lateral size: 5 μm (GNPs-20)), and multiwalled carbon nanotubes (Sigma-Aldrich Co., LLC., outer diameter × length: 6–13 nm × 2.5–20 μm (MWCNTs)). Prior to the pyrolytic process, we agitated the prepared reaction media at room temperature overnight to uniformly disperse the Pt $(acac)_2$ and sp^2 carbon materials. Subsequently, we heated the mixture at 573 K for 4 h and washed the resulting samples (Pt/GNPs-3, Pt/GNPs-20, and Pt/MWCNT) several times with anhydrous acetonitrile and dried them overnight in vacuum. We prepared specimens **1–6** under the six conditions described in Table 1. We used a commercially available Pt/C electrocatalyst (**Pt–C**, TEC10V30E, Tanaka Kikinzoku Kogyo Co., Ltd.) as the reference.

2.2 Characterization

We observed the morphologies of specimens **1–6** using a Hitachi H-7650 transmission electron microscope (TEM). We analyzed the amount of Pt nanoparticles loaded on the sp^2 carbon materials using inductively coupled plasma atomic emission spectroscopy (ICP-AES) (Shimadzu ICPS-7510). We evaluated the Brunauer–Emmett–Teller (BET) surface area using nitrogen adsorption–desorption analysis (Quantachrome Instruments). We characterized the original carbon materials and specimens **1–6** using a Nanophoton RAMANview Raman spectrometer.

2.3 Electrochemical measurements

We examined the electrocatalytic activities of specimens **1–6** using a computer-controlled Hokuto Denko HZ-7000 potentiostat/galvanostat. We obtained electrochemical measurements using a three-electrode cell with a 0.1 M $HClO_4$ aqueous solution. We used a glassy carbon rotating disk electrode (GC-RDE, surface area = 0.196 cm^2), Pt mesh electrode, and reversible hydrogen electrode (RHE) as the working, counter, and reference electrodes, respectively. We ionically connected the RHE to the electrolyte in the main cell compartment *via* a Luggin capillary tip positioned close to the working electrode (WE). Each sample prepared in this study was dispersed in an *i*-propanol solution with a weight concentration of 1.48 g L^{-1}. We added a 10 μL solution onto the GC-RDE (5 mm diameter) and allowed it to dry naturally. Finally, we covered the GC disk with 10 μL Nafion® *i*-propanolic solution (0.1 wt%) to fix the samples using a thin Nafion® layer. We conducted voltammetric experiments at 10 mV s^{-1} between 0.050 and 1.20 V (*vs.* RHE) at ~298 K. Prior to the experiments, we electrochemically cleaned the working electrode with 40–100 potential sweeps between 0.050 and 1.20 V at a scan rate of 50 mV s^{-1} under a N_2 atmosphere until the cyclic voltammograms (CVs) stabilized. Depending on the experimental

purpose, we deaerated the electrolyte by bubbling with N_2 or O_2 for at least 30 min.

We determined the electrochemical surface area (ECSA) of the Pt nanoparticles by hydrogen adsorption or desorption coulombic charge in the cyclic voltammogram under N_2 atmosphere after subtracting the double-layer charge current. We calculated the ECSA ($m^2\ g^{-1}$) using the following equation:

$$\mathrm{ECSA} = \frac{Q_H}{2.1 \times M_{Pt}} \quad (1)$$

where Q_H (C) is the charge of the hydrogen adsorption/desorption. An average value for the charge associated with a hydrogen adsorption/desorption monolayer formed on smooth polycrystalline Pt is 2.1 C m^{-2}.[30] M_{Pt} (g) is the Pt mass on the GC working electrode.

We investigated the ORR performance of the samples using rotating disk electrode linear sweep voltammetry (RDE-LSV) in the anodic direction at a sweep rate of 10 mV s^{-1} under five different RDE revolution speeds (200, 400, 800, 1200, and 1600 rpm) in an O_2 atmosphere. The resultant voltammograms were examined using the Koutecký–Levich equation.

$$\frac{1}{I} = \frac{1}{I_k} + \frac{1}{B\omega^{1/2}} \quad (2)$$

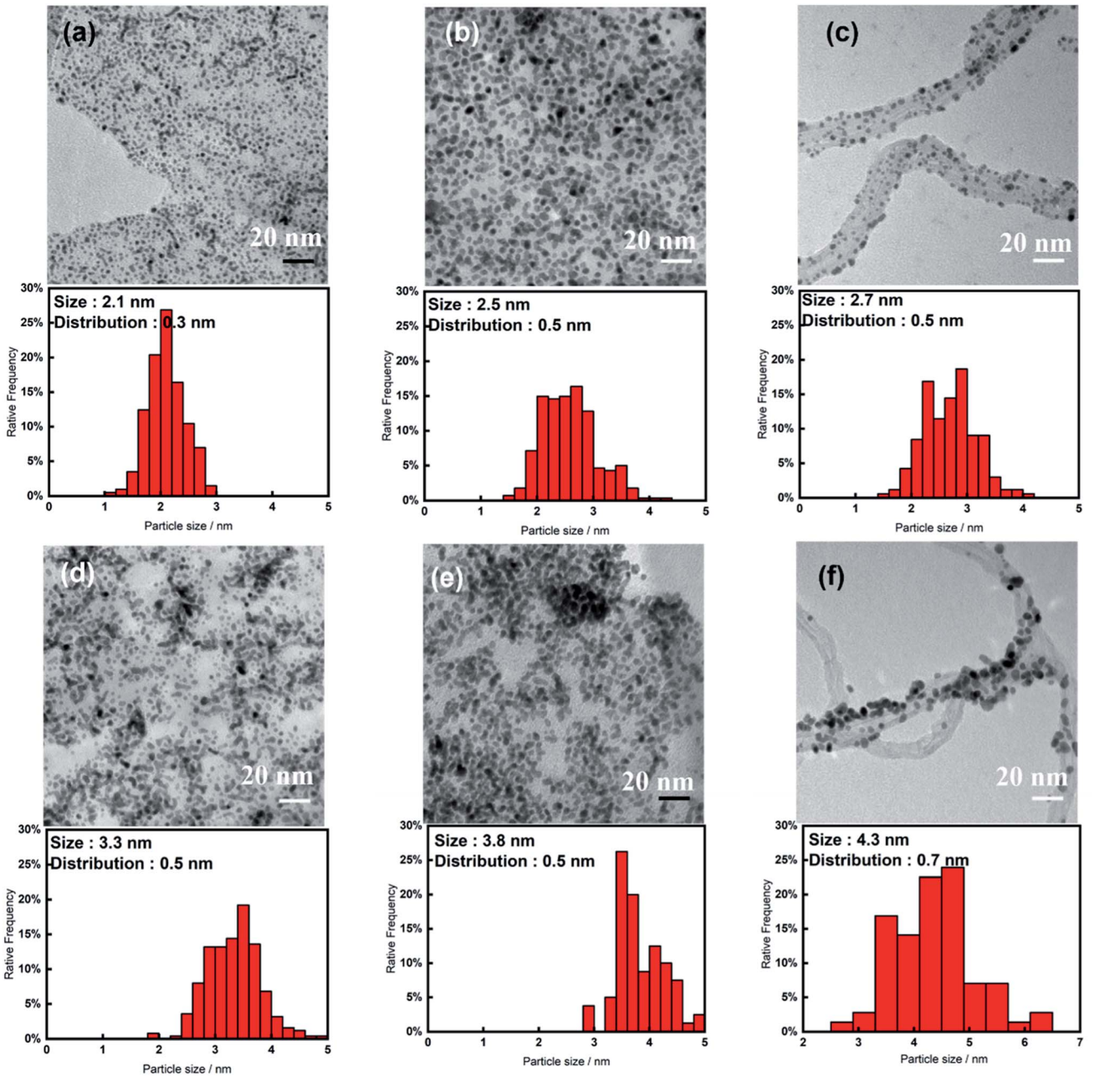

Fig. 1 TEM images and Pt nanoparticle size distribution of specimens (a–f) **1–6**, respectively, prepared under the experimental conditions described in Table 1.

$$B = 0.62nFAC^*D^{2/3}v^{-1/6}\omega^{1/2} \quad (3)$$

where I is the experimentally measured current at 0.85 V, I_k is the kinetically limited current, ω is the angular frequency of rotation (s^{-1}), n is the electron transfer number, F is the Faraday constant, A is the electrode surface area, C^* is the O_2 concentration in the electrolyte, D is the diffusion coefficient of O_2 in the electrolyte, and v is the kinematic viscosity of the electrolyte. We estimated I_k from the intercept of the Koutecký–Levich plot (I^{-1} *vs.* $\omega^{-1/2}$). For each catalyst, we normalized I_k to the Pt loading to obtain the mass activities.

We conducted the durability tests for the samples using the standard evaluation method recommended by the Fuel Cell Commercialization Conference of Japan.[31] This test overloads the cathode for a proton-exchange membrane (PEM) fuel-cell system by potential sweeps between 1.00 and 1.50 V (*vs.* RHE) at 500 mV s^{-1}, which easily causes the carbon support materials to corrode. Therefore, this electrochemical approach enables a quick durability evaluation of the cathode catalyst. To obtain further insight into the deterioration behavior, we estimated the catalytic activity retention rates for the ECSA and mass activities using the following equations:

$$\text{Catalytic activity retention rate for ECSA (\%)} = \frac{\text{ECSA estimated at each cycle } (m^2\ g_{Pt}^{-1})}{\text{initial ECSA } (m^2\ g_{Pt}^{-1})} \times 100 \quad (4)$$

$$\text{Catalytic activity retention rate for mass activity (\%)} = \frac{\text{mass activity estimated at each cycle } (A\ g_{Pt}^{-1})}{\text{initial mass acitvity } (A\ g_{Pt}^{-1})} \times 100 \quad (5)$$

3. Results and discussion

Fig. 1 shows the TEM images and Pt nanoparticle size distribution of specimens **1–6** that we prepared using the IL one-pot pyrolysis method under the conditions listed in Table 1. The ILs we used were $[C_4mim][Tf_2N]$ with an unsaturated five-membered ring cation with two heteroatoms and $[N_{1,1,1,3}][Tf_2N]$ with a saturated alkylammonium cation. The loading amounts of Pt and mean particle sizes of the nanoparticles deposited on the samples are summarized in Table 1. Regardless of the preparation conditions, the loading amounts were nearly the same (~25 wt%), but this was not the case for the mean particle size. For the graphene-nanoplatelets-based carbon supports, when we used the same IL, the Pt nanoparticles modified on GNPs-3 were smaller (2.1 nm for $[C_4mim][Tf_2N]$ and 3.3 nm for $[N_{1,1,1,3}][Tf_2N]$) than those on GNPs-20 (2.5 nm for $[C_4mim][Tf_2N]$ and 3.8 nm for $[N_{1,1,1,3}][Tf_2N]$). According to the product information, the specific surface area of GNPs-20 is 120–150 $m^2\ g^{-1}$.[32] A similar, flat, sheet-like, and ultrathin carbon material, GNPs-3, has a much larger specific surface area of 1243 $m^2\ g^{-1}$, which is calculated from the typical H3-type nitrogen adsorption–desorption isotherm curve of GNPs-3 (Fig. S2a (ESI†)). This higher specific surface area is extremely likely to result in smaller Pt nanoparticles, because GNPs-3 can provide more anchor points for Pt nucleation in the Pt(II) reduction process. However, the impact of specific surface area on Pt particle size seems to be limited, because the size variation is less than 0.5 nm even though the surface area is nearly 10 times larger. A schematic illustration of this plausible Pt nanoparticle formation mechanism is depicted in Fig. 2a and b. In addition, the geometric shape can affect the size of the nanoparticles. MWCNTs have completely different shapes but are sp^2 carbon materials, as are GNPs-3 and GNPs-20. Although the MWCNTs we used in this study had a higher surface area, *i.e.*, 210 $m^2\ g^{-1}$ (Fig. S2b (ESI†)), than GNPs-20, the Pt nanoparticles on the MWCNTs were slightly larger (2.7 nm for $[C_4mim][Tf_2N]$ and 4.3 nm for $[N_{1,1,1,3}][Tf_2N]$) than those on the GNPs-20. This result suggests that MWCNTs have fewer anchor points suitable for Pt nucleation. This may be associated with the curved surface shape of MWCNTs.

The difference in the IL species had a more noticeable effect on the Pt particle size in specimens **1–6**. As summarized in Table 1, the nanoparticles deposited became larger by changing the IL from $[C_4mim][Tf_2N]$ (specimens **1–3**) to $[N_{1,1,1,3}][Tf_2N]$ (specimens **4–6**). Nanoparticle growth in $[C_4mim][Tf_2N]$ was hampered. Similar behavior was also confirmed by Pt nanoparticle preparation using the same IL one-pot pyrolysis method but without carbon supports (Fig. S3 (ESI†)). The mean particle sizes of the Pt nanoparticles we obtained for $[C_4mim][Tf_2N]$ and $[N_{1,1,1,3}][Tf_2N]$ were 3.5 and 6.9 nm, respectively. Because the surface of the Pt nanoparticles prepared in ILs is positively charged, the Pt nanoparticles are considered to be stabilized by anionic supramolecular aggregates, for example, $[(\text{organic cation})_x(Tf_2N)_{1+x}]^-$.[33] In the present case, the accessibility of Pt metal precursors and/or atoms to the nanoparticle surface was directly controlled by the cationic steric effect.[34] Thus, a larger volume cation, $[C_4mim]^+$, could effectively block further Pt deposition on the nanoparticles. As a result, Pt nucleation was stimulated at other anchor points on the carbon supports, leading to less nanoparticle growth. A plausible process of Pt nanoparticle growth during the IL one-pot pyrolysis method is schematically summarized in Fig. 2c.

We collected further information on the carbon structure using Raman spectroscopy for specimens **1–6**, and the as-prepared samples are shown in Fig. S4 (ESI†). Two characteristic peaks, the D band at 1350 cm^{-1} and G band at 1580 cm^{-1}, are associated with defects or disorders and sp^2-bonded carbons, respectively.[35] We noted little difference between the Raman spectra before and after the Pt nanoparticle modification, indicating that the IL one-pot pyrolysis method employed in this research had no effect on the surface structure of the sp^2 carbon materials.

As expected from the characterization of the specimens, their electrochemical performance differed significantly. Fig. 3 shows the cyclic voltammograms before and after 15 000 potential cycle durability tests recorded at the GC electrodes with specimens **1–6** prepared by the one-pot pyrolysis method in a N_2-saturated 0.1 M $HClO_4$ aqueous solution. The several commonly observed redox waves concerning the hydrogen and oxygen electrochemical reactions are recognized at potentials ranging from 0.10 to 0.35 V and 0.60 to 1.00 V, respectively. The ECSAs for specimens **1–6** estimated from the voltammograms

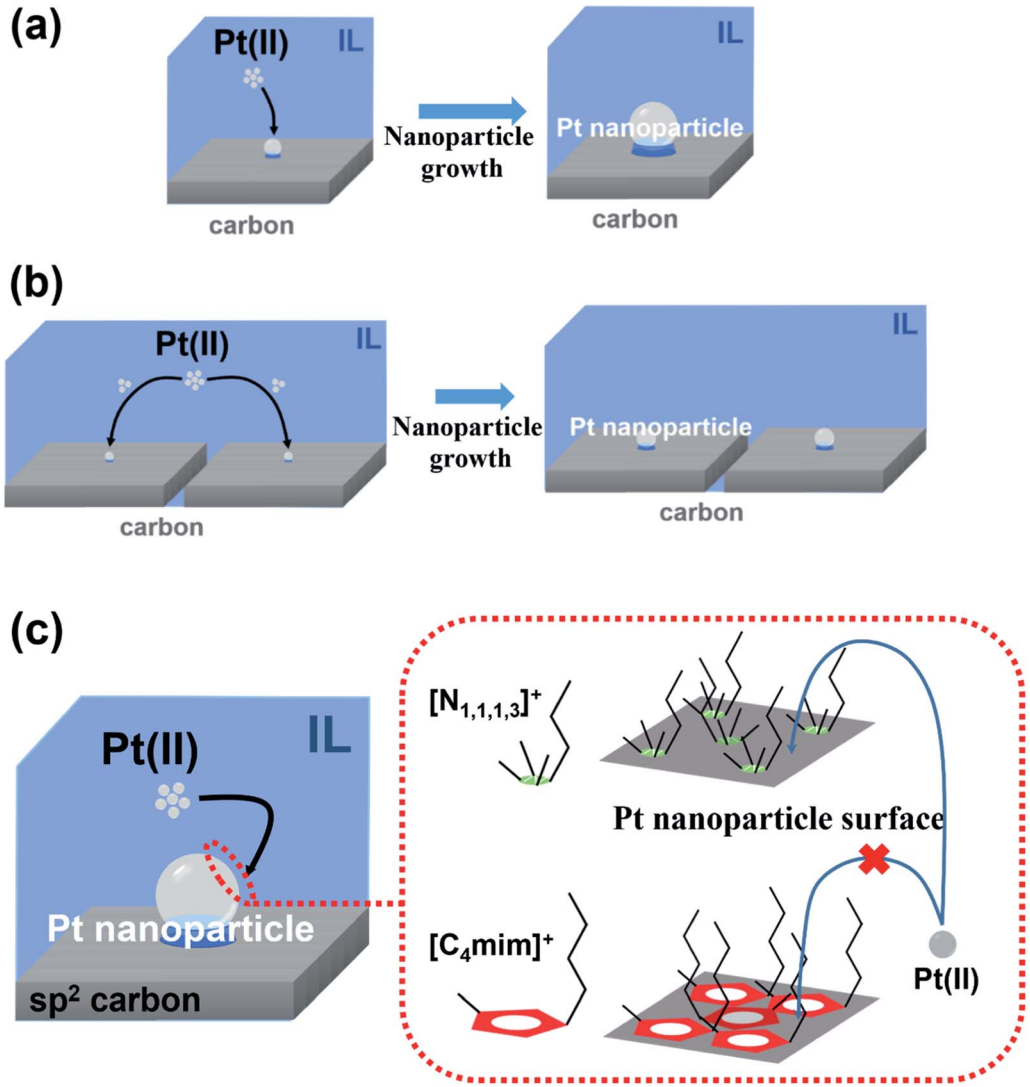

Fig. 2 Schematic illustration of the plausible impact of carbon materials with (a) smaller and (b) larger surfaces and (c) the organic cationic species in $[N_{1,1,1,3}][Tf_2N]$ and $[C_4mim][Tf_2N]$ on Pt nanoparticle size in the process of the IL one-pot pyrolysis method.

for hydrogen adsorption–desorption are shown in Table 2. These values are lower than those of commercial **Pt–C** catalysts. The H_2 adsorption was highly likely hampered by the IL remaining on the Pt nanoparticle surface.[36–38] After the durability test, we found that the ECSA retention rates for the graphene nanoplatelet-based samples, **1** (51.2%), **2** (47.6%), **4** (26.9%) and **5** (65.2%), were inferior to that of **Pt–C** (71.1%). Conversely, specimens **3** (75.1%) and **6** (92.8%), prepared using MWCNTs, showed higher retention rates than **Pt–C**. Considering the larger number of defects or disorders on the MWCNTs, corroborated by the Raman spectra derived from the G-band (Fig. S4 (ESI†)), we deduced that their presence triggered slower nanoparticle aggregation during the durability test, that is, a higher retention rate of ECSA by Pt/MWCNTs.

To evaluate the catalytic ability of specimens **1–6** toward the ORR, we measured the RDE-LSVs at the GC-RDEs with each specimen in an O_2-saturated 0.1 M $HClO_4$ aqueous solution before and after 15 000 potential cycle durability tests (Fig. S5 (ESI†)). Before the durability test, the increase in current flow for O_2 reduction initiated at *ca.* 1.05–1.10 V, as observed for commonly used electrocatalysts for the ORR. Koutecký–Levich plots at 0.85 V were constructed using the RDE-LSVs obtained at speeds of 200–1600 rpm. The mass activities of the specimens that we calculated from the Koutecký–Levich plots and the mean Pt particle sizes before the durability tests are summarized in Table 2 and Fig. 4. The mass activity decreased with increasing nanoparticle size. We obtained the highest mass activity, 329.9 A g^{-1}, for specimen **1**, which had the smallest mean nanoparticle size of 2.1 nm, corresponding to the size that can obtain more Pt (111) facets.[39] As focusing on Pt/GNPs-3 and Pt/GNPs-20, which are flat, sheet-like carbon supports, would provide an opportunity to discuss the effect of Pt nanoparticle density on catalytic ability, we prepared two extra GNPs-20-based specimens by the same procedure using $[N_{1,1,1,3}][Tf_2N]$

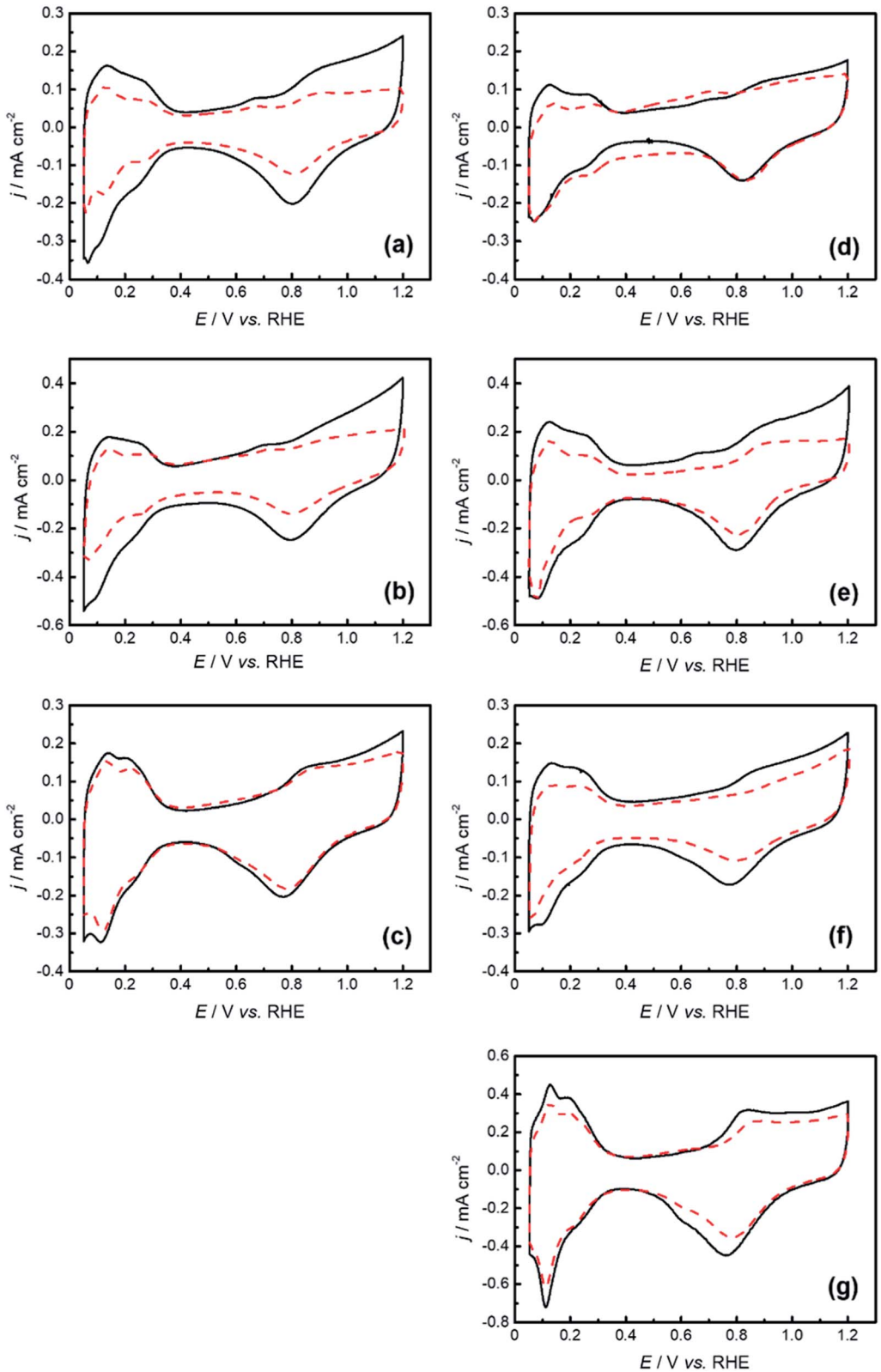

Fig. 3 Cyclic voltammograms recorded at glassy carbon electrodes with the specimens (a) **1**, (b) **2**, (c) **3**, (d) **4**, (e) **5**, and (f) **6** and (g) **Pt–C** in a N_2-saturated 0.1 M $HClO_4$ aqueous solution (—) before and (**- - -**) after the durability test. Scan rate was 10 mV s^{-1}.

Table 2 Summary of ECSA and mass activity data for specimens **1–6** and **Pt–C**

Specimens	ECSA (original)/ $m^2\ g^{-1}$	ECSA (after)/ $m^2\ g^{-1}$	Retention rate of ECSA/%	MA[a] @ 0.85 V (original)/A g^{-1}	MA[a] @ 0.85 V (after)/A g^{-1}	Retention rate of MA[a] @ 0.85 V/%
1	31.1	15.9	51.2	329.9	243.4	73.79
2	26.1	12.4	47.6	221.7	137.4	61.99
3	35.4	26.6	75.1	177.5	173.1	97.52
4	16.7	4.49	26.9	205.3	172.9	84.20
5	45.1	29.4	65.2	202.5	189.4	93.52
6	33.7	31.3	92.8	190.9	265.4	139.02
Pt–C	72.7	51.7	71.1	561.2	283.8	49.64

[a] MA: mass activity.

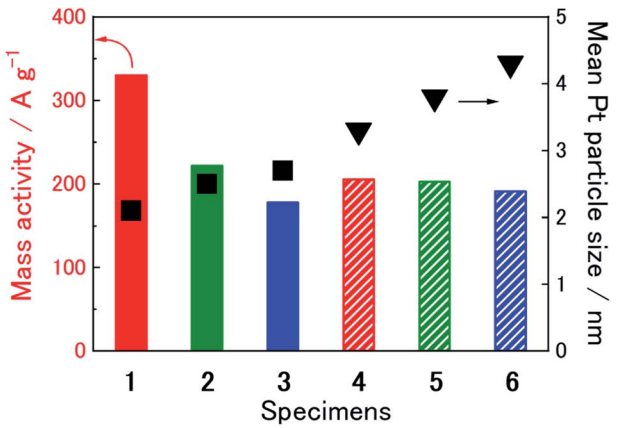

Fig. 4 Comparison of mass activity and mean Pt nanoparticle size of specimens **1–6**.

but with different Pt precursor concentrations of 1 and 2.5 mmol L^{-1}. TEM observation of the GNPs-20 prepared with 1, 2.5, and 5 mmol L^{-1} $Pt(acac)_2$ revealed that the mean particle sizes were 3.8 ± 0.6 nm, 3.6 ± 0.7 nm and 3.8 ± 0.5 nm, respectively (Fig. 5). In other words, size does not depend on the precursor concentration. However, the Pt loading varied with precursor concentration. From these findings, we concluded that the number density of Pt nanoparticles on GNPs-20 increases with increasing precursor concentration. The mass activities of these three specimens are shown in Fig. 6a as a function of Pt loading. The mass activities increase with increasing Pt loading, but are nonlinear. Because their particle sizes are almost the same, the differences in their mass activities are not dependent on size. This nonlinear behavior should be linked to the number density of the Pt nanoparticles on the GNPs-20. Watanabe *et al.* reported that the active area territory on the Pt surface is an important factor in attaining higher mass activity.[40] As illustrated in Fig. 6b, oxygen accessibility reduced when the Pt nanoparticle number density was too high.

Based on the RDE-LSVs after the 15 000-cycle tests (Fig. S5 and S6 (ESI†)), the mass activity data estimated at 0.85 V for specimens **1–6** and **Pt–C** are provided in Table 2. A comparison of all the mass activity data obtained in this study, with the catalytic activity retention rates, is presented in Fig. 7. All the specimens prepared showed a higher mass activity retention rate than **Pt–C** (49.6%). In particular, specimens **3** and **6**, resulting from the MWCNTs, showed a much higher durability. The results of Raman spectroscopy indicated that, as more functional groups exist on MWCNTs than on the other two sp^2 carbon materials, MWCNTs would suppress the displacement and aggregation of the Pt nanoparticles. Although the catalyst durability is improved by the IL binding between the Pt nanoparticles and the carbon material surface, the results here provide evidence that the original carbon surface properties also affect durability.

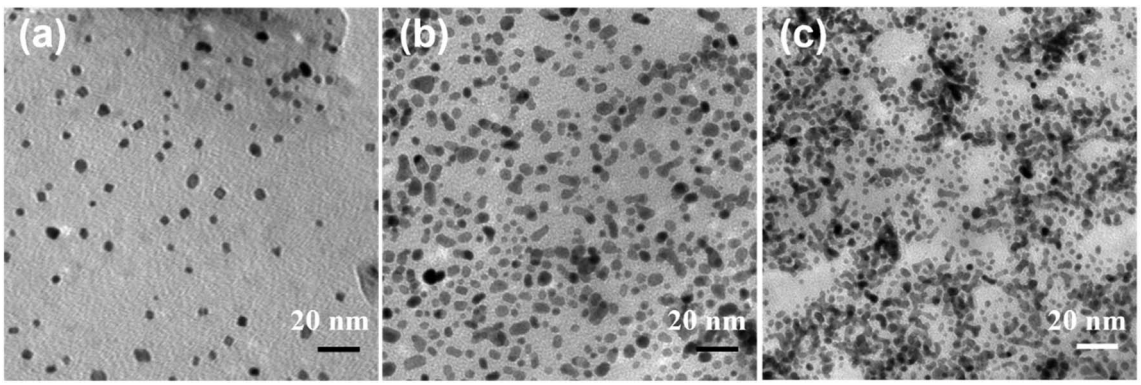

Fig. 5 TEM images of the Pt/GNPs-20s prepared in $[N_{1,1,1,3}][Tf_2N]$ with different Pt metal precursor ($Pt(acac)_2$) concentrations: (a) 1, (b) 2.5, and (c) 5 mmol L^{-1}.

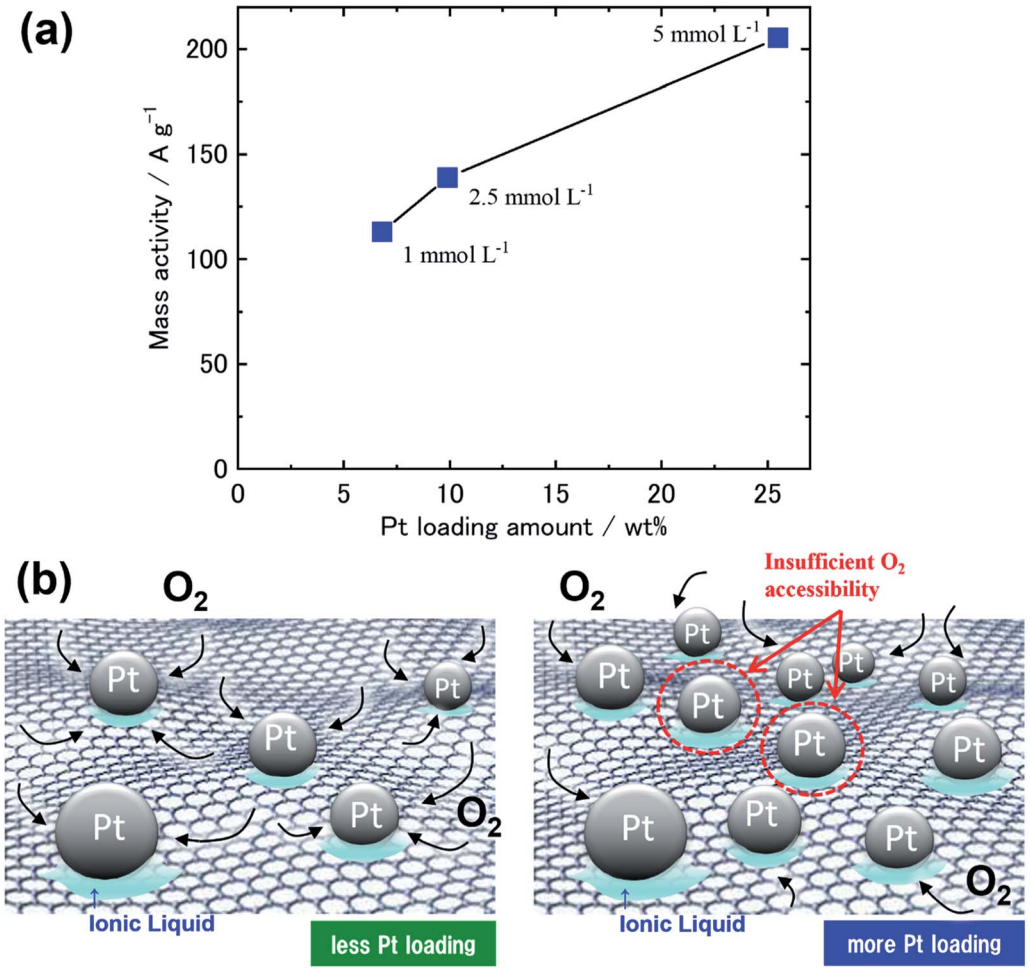

Fig. 6 (a) Comparison of mass activities with different Pt loading amounts on Pt/GNPs-20s prepared in $[N_{1,1,1,3}][Tf_2N]$ with different Pt metal precursor ($Pt(acac)_2$) concentrations: 1, 2.5, and 5 mmol L^{-1}. Pt particle size remained almost the same. (b) Schematic illustration of the effect of Pt nanoparticle number density deposited on GNPs-20s on mass transfer of oxygen during ORR.

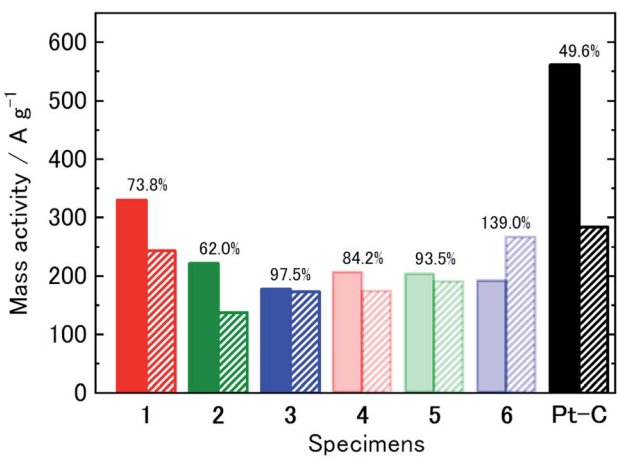

Fig. 7 Comparison of mass activity and mean Pt nanoparticle size of specimens **1–6** and **Pt–C**: (filled bar) before and (diagonal bar) after 15 000-cycle test.

4. Conclusions

In this study, we successfully synthesized Pt-nanoparticle-modified sp^2 carbon materials by the IL one-pot pyrolysis method using three different sp^2 carbon supports, GNPs-3, GNPs-20, and MWCNTs, without any pretreatment. The higher surface area of the carbon supports led to the formation of smaller Pt nanoparticles. The cation size in the IL also significantly affected the Pt nanoparticle size. We obtained the highest mass activity when the Pt nanoparticle size was ~2 nm. All the resulting specimens showed higher durability in terms of mass activity than the commercial catalyst. The samples prepared from MWCNTs had a much higher retention rate. More defects on the MWCNTs resulted in a stronger ability to fix the nanoparticles and prevent nanoparticle aggregation. This study provides useful information on the IL one-pot pyrolysis method for the synthesis of ORR electrocatalysts with high activity and durability.

Author contributions

T. T. conceived the idea of the one-pot process used in this research. S. K. gave the suggestions on experimental plan. Y. Y., Q. X. M. K. and H. Y. prepared and evaluated the specimens. Y. Y. and T. T. wrote the manuscript. All the authors participated in discussions of the results and in preparing the manuscript.

Conflicts of interest

The authors have no conflicts to declare.

Acknowledgements

This research was supported by JSPS KAKENHI (grant number JP19H02814).

References

1 M. Blal, A. Benatiallah, A. NeÇaibia, S. Lachtar, N. Sahouane and A. Belasri, Contribution and investigation to compare models parameters of (PEMFC), comprehensives review of fuel cell models and their degradation, *Energy*, 2019, **168**, 182–199.

2 A. Kulkarni, S. Siahrostami, A. Patel and J. K. Norskov, Understanding Catalytic Activity Trends in the Oxygen Reduction Reaction, *Chem. Rev.*, 2018, **118**, 2302–2312.

3 R. M. Darling and J. P. Meyers, Kinetic Model of Platinum Dissolution in PEMFCs, *J. Electrochem. Soc.*, 2003, **150**, A1523–A1527.

4 P. J. Ferreira, G. J. la O', Y. Shao-Horn, D. Morgan, R. Makharia, S. Kocha and H. A. Gasteiger, Instability of Pt/C Electrocatalysts in Proton Exchange Membrane Fuel Cells, *J. Electrochem. Soc.*, 2005, **152**, A2256–A2271.

5 X. Wang, W. Z. Li, Z. W. Chen, M. Waje and Y. S. Yan, Durability investigation of carbon nanotube as catalyst support for proton exchange membrane fuel cell, *J. Power Sources*, 2006, **158**, 154–159.

6 J. J. Wang, G. P. Yin, Y. Y. Shao, S. Zhang, Z. B. Wang and Y. Z. Gao, Effect of carbon black support corrosion on the durability of Pt/C catalyst, *J. Power Sources*, 2007, **171**, 331–339.

7 R. Borup, J. Meyers, B. Pivovar, Y. S. Kim, R. Mukundan, N. Garland, D. Myers, M. Wilson, F. Garzon, D. Wood, P. Zelenay, K. More, K. Stroh, T. Zawodzinski, J. Boncella, J. E. McGrath, M. Inaba, K. Miyatake, M. Hori, K. Ota, Z. Ogumi, S. Miyata, A. Nishikata, Z. Siroma, Y. Uchimoto, K. Yasuda, K. Kimijima and N. Iwashita, Scientific aspects of polymer electrolyte fuel cell durability and degradation, *Chem. Rev.*, 2007, **107**, 3904–3951.

8 S.-M. Jung, S.-W. Yun, J.-H. Kim, S.-H. You, J. Park, S. Lee, S. H. Chang, S. C. Chae, S. H. Joo, Y. Jung, J. Lee, J. Son, J. Snyder, V. Stamenkovic, N. M. Markovic and Y.-T. Kim, Selective electrocatalysis imparted by metal–insulator transition for durability enhancement of automotive fuel cells, *Nat. Catal.*, 2020, **3**, 639–648.

9 S. Sui, X. Y. Wang, X. T. Zhou, Y. H. Su, S. Riffatc and C. J. Liu, A comprehensive review of Pt electrocatalysts for the oxygen reduction reaction: Nanostructure, activity, mechanism and carbon support in PEM fuel cells, *J. Mater. Chem. A*, 2017, **5**, 1808–1825.

10 X. J. Zhou, J. L. Qiao, L. Yang and J. J. Zhang, A Review of Graphene-Based Nanostructural Materials for Both Catalyst Supports and Metal-Free Catalysts in PEM Fuel Cell Oxygen Reduction Reactions, *Adv. Energy Mater.*, 2014, **4**, 1301523.

11 Y. J. Li, Y. J. Li, E. B. Zhu, T. McLouth, C. Y. Chiu, X. Q. Huang and Y. Huang, Stabilization of High-Performance Oxygen Reduction Reaction Pt Electrocatalyst Supported on Reduced Graphene Oxide/Carbon Black Composite, *J. Am. Chem. Soc.*, 2012, **134**, 12326–12329.

12 J. H. Kim, J. Y. Cheon, T. J. Shin, J. Y. Park and S. H. Joo, Effect of surface oxygen functionalization of carbon support on the activity and durability of Pt/C catalysts for the oxygen reduction reaction, *Carbon*, 2016, **101**, 449–457.

13 D. Higgins, P. Zamani, A. P. Yu and Z. W. Chen, The application of graphene and its composites in oxygen reduction electrocatalysis: a perspective and review of recent progress, *Energy Environ. Sci.*, 2016, **9**, 357–390.

14 R. Kou, Y. Y. Shao, D. H. Mei, Z. M. Nie, D. H. Wang, C. M. Wang, V. V. Viswanathan, S. Park, I. A. Aksay, Y. H. Lin, Y. Wang and J. Liu, Stabilization of Electrocatalytic Metal Nanoparticles at Metal-Metal Oxide-Graphene Triple Junction Points, *J. Am. Chem. Soc.*, 2011, **133**, 2541–2547.

15 S. Liu, J. Wang, J. Zeng, J. Ou, Z. Li, X. Liu and S. Yang, "Green" electrochemical synthesis of Pt/graphene sheet nanocomposite film and its electrocatalytic property, *J. Power Sources*, 2010, **195**, 4628–4633.

16 L. Guo, W. J. Jiang, Y. Zhang, J. S. Hu, Z. D. Wei and L. J. Wan, Embedding Pt Nanocrystals in N-Doped Porous Carbon/Carbon Nanotubes toward Highly Stable Electrocatalysts for the Oxygen Reduction Reaction, *ACS Catal.*, 2015, **5**, 2903–2909.

17 D. Higgins, M. A. Hoque, M. H. Seo, R. Y. Wang, F. Hassan, J. Y. Choi, M. Pritzker, A. P. Yu, J. J. Zhang and Z. W. Chen, Development and Simulation of Sulfur-doped Graphene Supported Platinum with Exemplary Stability and Activity Towards Oxygen Reduction, *Adv. Funct. Mater.*, 2014, **24**, 4325–4336.

18 D. P. He, C. Zeng, C. Xu, N. C. Cheng, H. G. Li, S. C. Mu and M. Pan, Polyaniline-Functionalized Carbon Nanotube Supported Platinum Catalysts, *Langmuir*, 2011, **27**, 5582–5588.

19 T. Fujigaya and N. Nakashima, Fuel Cell Electrocatalyst Using Polybenzimidazole-Modified Carbon Nanotubes As Support Materials, *Adv. Mater.*, 2013, **25**, 1666–1681.

20 T. Tsuda, T. Kurihara, Y. Hoshino, T. Kiyama, K. Okazaki, T. Torimoto and S. Kuwabata, Electrocatalytic Activity of Platinum Nanoparticles Synthesized by Room-Temperature Ionic Liquid-Sputtering Method, *Electrochemistry*, 2009, **77**, 693–695.

21 T. Tsuda, K. Yoshii, T. Torimoto and S. Kuwabata, Oxygen reduction catalytic ability of platinum nanoparticles prepared by room-temperature ionic liquid-sputtering method, *J. Power Sources*, 2010, **195**, 5980–5985.
22 T. Fujigaya, S. Hirata and N. Nakashima, A highly durable fuel cell electrocatalyst based on polybenzimidazole-coated stacked graphene, *J. Mater. Chem. A*, 2014, **2**, 3888–3893.
23 K. Yoshii, T. Tsuda, T. Arimura, A. Imanishi, T. Torimoto and S. Kuwabata, Platinum nanoparticle immobilization onto carbon nanotubes using Pt-sputtered room-temperature ionic liquid, *RSC Adv.*, 2012, **2**, 8262–8264.
24 R. Izumi, Y. Yao, T. Tsuda, T. Torimoto and S. Kuwabata, Oxygen reduction electrocatalysts sophisticated by using Pt nanoparticle-dispersed ionic liquids with electropolymerizable additives, *J. Mater. Chem. A*, 2018, **6**, 11853–11862.
25 T. Sasaki, R. Izumi, T. Tsuda and S. Kuwabata, Innovative Approach for Preparing a CNT-Supported Pt Nanoparticle Functional Electrocatalyst Using Protic Ionic Liquids, *ACS Appl. Energy Mater.*, 2021, **4**, 7298–7308.
26 Y. Yao, R. Izumi, T. Tsuda, Y. Oshima, A. Imanishi, N. Oda and S. Kuwabata, Pt and PtNi nanoparticle-supported multi-walled carbon nanotube electrocatalysts prepared by one-pot pyrolytic synthesis with an ionic liquid, *ACS Appl. Energy Mater.*, 2019, **2**, 4865–4872.
27 T. S. Ahmadi, Z. L. Wang, T. C. Green, A. Henglein and M. A. ElSayed, Shape-controlled synthesis of colloidal platinum nanoparticles, *Science*, 1996, **272**, 1924–1926.
28 B. R. Cuenya, Synthesis and catalytic properties of metal nanoparticles: Size, shape, support, composition, and oxidation state effects, *Thin Solid Films*, 2010, **518**, 3127–3150.
29 Y. N. Xia, X. H. Xia and H. C. Peng, Shape-Controlled Synthesis of Colloidal Metal Nanocrystals: Thermodynamic versus Kinetic Products, *J. Am. Chem. Soc.*, 2015, **137**, 7947–7966.
30 K. Yamamoto, D. M. Kolb, R. Kotz and G. Lehmpfuhl, Hydrogen Adsorption and Oxide Formation on Platinum Single-Crystal Electrodes, *J. Electroanal. Chem.*, 1979, **96**, 233–239.
31 M. Asano, R. Kawamura, R. Sasakawa, N. Todoroki and T. Wadayama, Oxygen Reduction Reaction Activity for Strain-Controlled Pt-Based Model Alloy Catalysts: Surface Strains and Direct Electronic Effects Induced by Alloying Elements, *ACS Catal.*, 2016, **6**, 5285–5289.
32 **https://www.strem.com/catalog/v/06-0210/12/carbon_1034343-98-0**.
33 C. W. Scheeren, G. Machado, S. R. Teixeira, J. Morais, J. B. Domingos and J. Dupont, Synthesis and Characterization of Pt(0) Nanoparticles in Imidazolium Ionic Liquids, *J. Phys. Chem. B*, 2006, **110**, 13011–13020.
34 G. R. Zhang, T. Wolker, D. J. S. Sandbeck, M. Munoz, K. J. J. Mayrhofer, S. Cherevko and B. J. M. Etzold, Tuning the Electrocatalytic Performance of Ionic Liquid Modified Pt Catalysts for the Oxygen Reduction Reaction via Cationic Chain Engineering, *ACS Catal.*, 2018, **8**, 8244–8254.
35 P. Lespade, R. Al-Jishi and M. S. Dresselhaus, Model for Raman Scatterig From Incompletely Graphitized Carbons, *Carbon*, 1982, **20**, 427–431.
36 L. Johnson, A. Ejigu, P. Licence and D. A. Walsh, Hydrogen Oxidation and Oxygen Reduction at Platinum in Protic Ionic Liquids, *J. Phys. Chem. C*, 2012, **116**, 18048–18056.
37 G. R. Zhang, M. Munoz and B. J. M. Etzold, Boosting Performance of Low Temperature Fuel Cell Catalysts by Subtle Ionic Liquid Modification, *ACS Appl. Mater. Interfaces*, 2015, **7**, 3562–3570.
38 K. Huang, T. Song, O. Morales-Collazo, H. Jia and J. F. Brennecke, Enhancing Pt/C Catalysts for the Oxygen Reduction Reaction with Protic Ionic Liquids: The Effect of Anion Structure, *J. Electrochem. Soc.*, 2017, **164**, F1448–F1459.
39 M. Shao, A. Peles and K. Shoemaker, Electrocatalysis on Platinum Nanoparticles: Particle Size Effect on Oxygen Reduction Reaction Activity, *Nano Lett.*, 2011, **11**, 3714–3719.
40 M. Watanabe, H. Sei and P. Stonehart, The Influence of Platinum Crystallite Size on the Electroreduction of Oxygen, *J. Electroanal. Chem. Interfacial Electrochem.*, 1989, **261**, 375–387.